RSC Advances

PAPER

View Article Online
View Journal | View Issue

Cite this: RSC Adv., 2017, 7, 39292

A "hairy" polymer/3D-foam hybrid for flexible high performance thermal gap filling applications in harsh environments†

M. Loeblein,[ab] L. Jing,[c] M. Liu,[cd] J. J. W. Cheah,[cd] S. H. Tsang[b] and E. H. T. Teo*[ac]

Received 6th June 2017
Accepted 19th July 2017

DOI: 10.1039/c7ra06297d

rsc.li/rsc-advances

Thermal management in harsh environment electronics (*i.e.* automotive, avionics, oil and gas industry) has become a latent problem. Due to the more stringent requirements of the materials, such as higher operating temperatures, ability to operate under exposure to vibration and shock, and over larger gaps with complex paths, and increased demands in terms of reliability, the solutions adopted for consumer electronics cannot be directly translated into these applications and the current materials and approaches used are reaching their limits. Herein we present a new polymer/3D-foam composite that can fill large gaps and retain a thermal conductivity of 62–86 W m^{-1} K^{-1}, while providing strong mechanical support with a strong restorative force (*i.e.* can withstand vibration). At the same time, it is demonstrated to have a superior surface conformity to usual gap fillers and is able to remain stable up to temperatures as high as 330 °C, which is ∼180 °C higher than current conventional packaging materials.

Open Access Article. Published on 10 August 2017. Downloaded on 7/31/2024 8:21:09 AM.
This article is licensed under a Creative Commons Attribution-NonCommercial 3.0 Unported Licence.

Introduction

Similarly to consumer electronics,[1,2] electronics in the automotive environment (ambient temperatures from −40° to +200 °C)[3,4] and other harsh environments, such as in the downhole oil and gas industry (with operating temperatures up to +150 °C and +200 °C, respectively) and avionics industry (with ambient temperatures from −55 °C to +200 °C)[5] are experiencing higher demands in performance (*i.e.* faster processors, more functions, higher bandwidths) while becoming more compact and smaller.[6,7] This leads to a drastic increase in power densities and heat dissipation rates (*e.g.* values as high as 100 W cm^{-2} for commercial and 1000 W cm^{-2} for military high power electronics are soon to be reached).[8] With these changes, the thermal management problem in those fields has also become increasingly severe.[6] Despite the improvement achieved for thermal management solutions in consumer electronics,[9–11] those thermal solutions cannot be directly applied for harsh environment applications, since the gaps to be filled are thicker (in the order of millimetres, which is much larger than that of thermal interface materials (TIMs) used in electronic device applications), sometimes complexly wound in random directions,[12] the ambient and operating temperatures are higher and additional exposure to shock, vibration and sometimes even spillage are common additional difficulties encountered.[4–6]

One prominent example that highlights the increasing thermal management challenge in harsh environments are batteries and fuel cells in electric vehicles: it is imperative that they operate effectively in all climates and they must maintain an optimum average temperature with even temperature distribution; but at the same time the demand on higher storage capacity is steadily increasing, while charging times, size and weight have to decrease.[13,14] This bears heavily on the power dissipation and design.[7] The thermal management system must thus improve, while remaining compact, lightweight, low cost, easily packaged and compatible with the location in the vehicle.[15] Furthermore, it must be compatible with high-volume production (for approximately 55 million vehicles sold in the world per year),[4] and fulfil long-term reliability requirements (*i.e.* need to survive 2000–2500 thermal cycles with <1% which is the reliability demand of vehicles for 10 years, which is about 241 350 km or 150 000 miles).[16] Normal packaging materials used are only robust up to 150 °C and are unable to reliably withstand the severe shock and vibration experienced.[4,17] The use of alternative thermal management systems like fans and water cooling add weight and cost or are incompatible with the location and design of the vehicle.[6]

In order to mitigate the thermal challenge of electronics, we recently developed a new class of nano-TIM, 3D-foams, and demonstrated great enhancement of thermal conductivity through compression (reaching thermal conductivity values of 62–86 W m^{-1} K^{-1}), high surface conformity and outstanding

[a]School of Electrical and Electronic Engineering, Nanyang Technological University, 50 Nanyang Avenue, Singapore 639798, Singapore. E-mail: HTTEO@ntu.edu.sg
[b]CNRS-International NTU Thales Research Alliance (CINTRA), UMI 3288, Research Techno Plaza, 50 Nanyang Drive, Singapore, Singapore 637553
[c]School of Material Science and Engineering, Nanyang Technological University, 50 Nanyang Avenue, Singapore 639798, Singapore
[d]Temasek Laboratories@NTU, 50 Nanyang Avenue, Singapore 639798, Singapore

† Electronic supplementary information (ESI) available: Fig. S1–S4. See DOI: 10.1039/c7ra06297d

This journal is © The Royal Society of Chemistry 2017

Open Access Article. Published on 10 August 2017. Downloaded on 7/31/2024 8:21:09 AM.
This article is licensed under a Creative Commons Attribution-NonCommercial 3.0 Unported Licence.

performance on field (20–30% improvement over state-of-the-art TIMs, with achieved temperature decreases by ΔT of 44–24 °C).[18] These 3D-foams are a class of interconnected networked structure that comprises of multilayer domains of 2D-graphene and hexagonal boron nitride (h-BN).[19,20] They retain the intrinsic properties of their 2D-constituents (such as high thermal conductivity, electrical conductivity, chemical inertness), while greatly enhancing surface area and mechanical robustness.[21,22] Despite these improvements, their use for gap filling applications is limited, due to the compressibility of the 3D-foams which confines the final thickness achievable down to the μm range.

One way to achieve increased thickness is by infusing the 3D-foams with polymers. The polymer backbone provides a robust support for the 3D-foam and enhances flexibility, allows easier handling and prevents the 3D-foam from total compression.[19,23] Even though there have already been reports on the infiltration of 3D-foams with polymers for thermal-related applications,[24–26] the obtained results show a drastic decrease of electrical conductivity and thermal properties of the 3D-foams (*i.e.* none of the reported values is nearly the 60 W m^{-1} K^{-1} of the bare compressed foam). More compelling, additional layers of bare polymer below the structure are inevitable using typical polymer-infusion techniques, which further lowers the performance and does not provide good surface conformity properties.[27] Mitigating this problem by increasing the filling fraction of the foam is often not successful, since the achieved further increase in thermal conductivity is minimal[28] and it can yield to loss of flexibility of the polymer.[29]

In order to address all these issues, in this work we developed a new way of infusion of 3D-foams with polymer, which combines the advantages of both: the infusion process provides mechanical support, while at the same time the intrinsic properties of the 3D-foam as well as its surface conformity are fully preserved. The principle used relies in infusing only the central layer of the foam, as schematized in Fig. 1. We call this infusion process the "hairy" method.

Since in automotive applications elastomeric polymers of silicone (such as polydimethylsiloxane, PDMS) are already used in mountings around motor coils of electric vehicles,[12] PDMS is the choice of polymer for this work. Results show that this technique fully preserves the structure and quality of the 3D-foam at its exposed parts. The overall thermal conductivity of the structure fully achieves the 62–86 W m^{-1} K^{-1} of bare 3D-foams and the electrical properties are also fully preserved. The tensile strength of the foam is increased nearly 3-fold, the elongation 57-fold and compression studies demonstrated that the foam can work as potential robust large gap filler with 90% recoverability. In a last step, the stability at high temperatures was assessed, which confirmed the suitability of this structure for harsh environment.

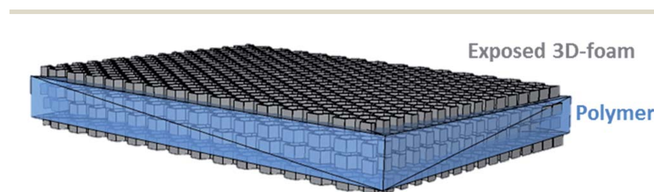

Fig. 1 Schematic of the "hairy" structure of 3D-foam in polymer.

Experimental

Sample preparation

3D-foams are grown using thermal chemical vapour deposition (CVD).[21] In brief, Ni foam is used as a catalytic substrate and annealed to remove oxidation and expand its grain size. For 3D-graphene (3D-C) this is done for 5 min under Ar and H_2 environment, for 3D-boron nitride (3D-BN), under low pressure with H_2 for 2 h. Afterwards, the precursor gas is led into the chamber to start the growth. For 3D-C, the precursor gas is CH_4, for 3D-BN sublimated ammonia-borane powder. Growth of 3D-C is terminated after 10 min, for 3D-BN after 1 h. After fast cool down, the samples are taken out of the furnace and the "hairy" infusion step (Fig. 2) is performed: first, a thin layer of polycaprolactone diol is melted at 80 °C in an aluminium pan, then the 3D-C/BN coated Ni foam dipped into the melt to coat the edge with a thin layer of polycaprolactone diol. The height of the molten polycaprolactone diol inside the pan determines the thickness of the later exposed part of 3D-foam. Subsequently the pan with the foam inside is quenched in ice bath to solidify the polycaprolactone diol layer on the surface of the 3D-foam. The same procedure is repeated for the other side. This yields a porous 3D-foam sandwiched between two thin layers of polycaprolactone diol. Polycaprolactone diol is specifically chosen for these protective steps since it has a suitable viscosity, a higher melting temperature than the curing temperature used for PDMS and since it is relatively easy to remove from the protected foam areas once the PDMS is cured, without damaging the underlying 3D-foam. In a next step, PDMS is subsequently infused into the remaining uncoated layers of the foam to obtain a uniform coating of PDMS within the porous structure. Degassing is carried out during infusion process to remove air bubbles and ensure a uniform coating throughout the 3D-foam. The PDMS coated foam is left in the oven at 60 °C for 24 h. Afterwards, the polycaprolactone diol is dissolved and rinsed a few times in cyclohexane to fully remove traces of polycaprolactone diol in the system, exposing the hairy

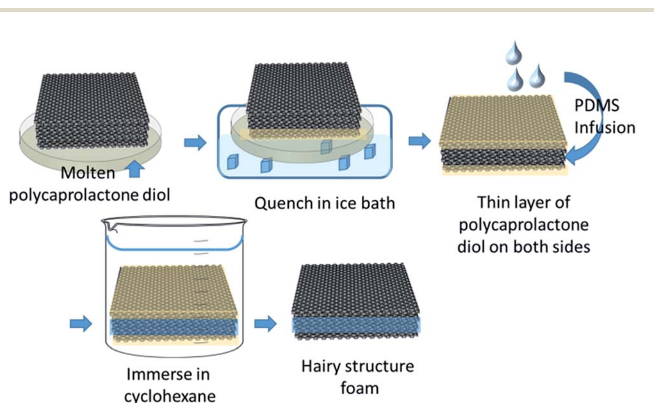

Fig. 2 Schematics of the "hairy" infusion of 3D-foams with PDMS.

Open Access Article. Published on 10 August 2017. Downloaded on 7/31/2024 8:21:09 AM.
This article is licensed under a Creative Commons Attribution-NonCommercial 3.0 Unported Licence.

structure of the original foam. The samples used for testing herein were prepared with a 50 vol% coating with PDMS (*i.e.* initial thickness of the 3D-foam is of 2 mm, the central PDMS layer is of 1 mm thickness). Once the samples are completely dry, the Ni is etched away through chemical etching with HCl. After all the Ni is removed, samples are washed in DI-H_2O and subsequently dried.

For comparison "conventional" PDMS-filled samples are also prepared by dripping the same PDMS matrix onto the entire 3D-foam/Ni structure (without any polycaprolactone diol coating), followed by curing for 24 h at 60 °C and subsequent etching of Ni using the same HCl etchant.

Characterization

For optical imagining, scanning electron microscopy (SEM, JEOL JSM-IT100 at 15 kV) was used. Raman spectroscopy (WITec CRM200 Raman with an Nd:YAG 532 nm laser as excitation source) was performed at room temperature to determine the crystalline configuration of the 3D-foams before and after the infusion. Electrical conductivity was measured using the 4-point van der Pauw method,[30] thermal conductivity using the laser flash method.[31] For both these measurements the "hairs" were compressed down to the PDMS central layer, as this would be the configuration used in thermal gap filling application (as schematized in Fig. 3). In this "working condition" an improved contact can be achieved, as well as high thermal conductivity.

To evaluate the mechanical properties, Instron® 5567 mechanical tester system at room temperature in tensile and compression mode was used. For tensile testing, samples of known dimensions were clamped and then a strain rate of 1 mm min^{-1} applied. Tensile stress and strain are determined from the applied tensile force over the original specimen cross-sectional area and elongation of the sample over its original length, respectively. For compression testing, the sample with a specified dimension was loaded at the center of the lower platen; a compression rod with 50 mm diameter was then applied onto the sample with a controlled speed. All the compressions were conducted within the confinement of the small upper platen. Compressive strain and stress were calculated using the displacement of the compression rod divided by the original height of the sample and the applied compressive force over the cross-sectional area of the samples, respectively. Recoverability of the sample is defined as the displacement recovered over applied displacement. The cyclic uniaxial compression experimental data was acquired at a loading–unloading rate of 0.04 mm min^{-1} at a strain of 60%. For the "hairy" sample, the exposed bare 3D-foam was already pre-compressed, since this is the configuration in the final application of gap filler. A total of 100 compression cycles were performed for the "hairy" 3D-foam, 10 cycles for the bare 3D-foam.

To determine the high temperature stability of the "hairy" foams, thermogravimetric analysis (TGA, Shimadzu Scientific Instruments DTG-60H) was performed. This method assesses the decomposition profile of the material by heating it up to ~1100 °C while monitoring the weight.[32,33] This way, any changes in physical and chemical properties of the material tested are measured as a function of increasing temperature.

Results and discussion

Fig. 4a and b show optical images of the obtained samples with and without the PDMS infusion. It can be seen that the process does not change the overall physical appearance of the 3D-foams. In Fig. 4c and d the flexibility of the structures is demonstrated, as they are able to completely conform to the curvature of a 6.5 mm diameter rod and fully return back to their original shape without breaking. This is in big contrast to bare 3D-foams, which beyond a bending angle of 15° immediately break (Fig. S1, ESI†). Cross-sectional SEM images of the 3D-foams without and with the "hairy" infusion are shown in Fig. 4e and f, respectively. It can be seen clearly that the infusion yields a single thin layer of PDMS in the centre of the foam without causing any contamination, and without causing any structural changes to the 3D-foams (*i.e.* their structure outside the infusion layer remains intact, exactly like the 3D-foam's bare morphology). Comparative optical images and SEM images of the conventional PDMS infusion of 3D-foams are shown in Fig. S2 and S3, respectively, in the ESI.†

Further corroboration of the non-invasiveness (*i.e.* no changes in quality) was assessed through Raman spectroscopy, and results are shown in Fig. 5. As evident from the graphs, the infusion step does not alter the crystal structure of the 3D-foams, since the position and width of all the characteristic

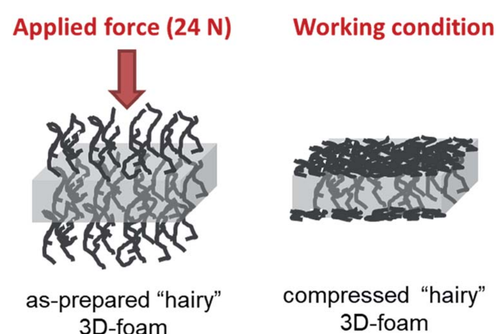

Fig. 3 Schematic of the working condition of the "hairy" foam for gap filling applications.

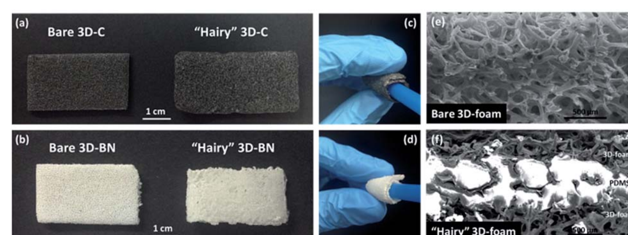

Fig. 4 Optical images without and with the PDMS "hairy" infusion of (a) 3D-C and (b) 3D-BN. Demonstration of flexibility of (c) "hairy" 3D-C and (d) "hairy" 3D-BN. Cross-sectional SEM images of (e) bare 3D-foam and (f) "hairy" 3D-foam.

 This journal is © The Royal Society of Chemistry 2017

Open Access Article. Published on 10 August 2017. Downloaded on 7/31/2024 8:21:09 AM.
This article is licensed under a Creative Commons Attribution-NonCommercial 3.0 Unported Licence.

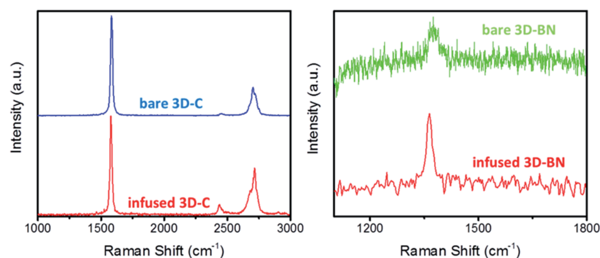

Fig. 5 Raman spectroscopy results on bare 3D-foams and 3D-foams with "hairy" infusion.

peaks of graphene and h-BN remain unchanged (*i.e.* for 3D-C, G-peak at 1580 cm^{-1}, 2D-peak at 2700 cm^{-1} and absence of D-peak; for 3D-BN, h-BN peak at 1370 cm^{-1}).[34,35]

To quantify the enhancement of mechanical performance with this novel "hairy" method, uniaxial tensile and compression tests *via* Instron® mechanical tester were performed on the "hairy" 3D-foam, and same tests were also carried out on bare 3D-foam for comparison. The corresponding stress–strain curves are shown in Fig. 6. Fig. 6a shows the representative tensile stress–strain curves of the hairy 3D-foam and bare 3D-foam. It can be observed that all the samples follow similar trajectories, *i.e.* linear mechanical behaviour (stress–strain relationship) until an abrupt breaking point. The inset in Fig. 6a shows an enlarged graph of the bare 3D-foam tensile stress–strain curve. It can be seen that there are several peaks and valleys along the curve, which was previously assigned to the alignment of single graphene branches within 3D-C towards the direction of the tensile load.[36] Here, this was also observed for the tensile curves of 3D-BN. It can be seen that the hairy 3D-foam performs with much higher breaking elongation as compared to the bare 3D-foam. The as prepared bare 3D-foam exhibits high Young's modulus of 10.5 MPa on account of the intrinsically strong graphene domain (graphene has a Young's Modulus of 1050 GPa),[37] while it breaks at the strain as low as 1.8%, which is due to the weak van der Waals stacking between the domains[21] that uncouples easily upon tensile loading. While for the hairy 3D-foam, the almost two orders increased breaking elongation at 102% is even higher as compared to the bare PDMS and conventional 3D-foam/PDMS (ESI Fig. S4†). This large increase in strain-at-break is not only attributed to the highly crosslinked PDMS chains within the structure which can endure high tensile load,[38] but also due to additional free interactions (frictions) between the PDMS chains and the graphene domains, which lead to timely dissipation of energy accumulated during the tensile loading, postponing the stress concentration induced failure. As a result, the well-connected 3D structure and the high intrinsic mechanical structure of the graphene domains[36] contribute to the increases of both tensile strength (from 0.19 to 0.54 MPa, 3-fold increase) and breaking elongation. The remarkable tensile mechanical performance of the hairy 3D-foam indicates its outstanding flexibility and toughness, which are pivotal for its potential applications.

To demonstrate the robustness of the "hairy" 3D-foams for gap filler application, cyclic compression tests were also carried out to study their responses upon compressive loading. Fig. 6b shows representative stress–strain curves of the bare 3D-foam and the hairy 3D-foam at an applied strain of 60%. It can be observed that an almost full shape recovery is performed for the hairy 3D-foam after first loading–unloading cycle, which remains consistent over the long-term compression of up to 100 cycles, showing no observable degradations in shape recovery characteristics and properties and compressive strength. With only 50% of the total volume of the sample with PDMS, the "hairy" 3D-foam was able to perform with a comparable shape recoverability as compared to bare PDMS, which makes it capable of providing stable mechanical support when serving as thermal gap filler. Contrastingly, the bare 3D-foam deforms almost plastically upon continuous compression with only 16% shape recoverability (inset of Fig. 6b) after first compression at a 60% strain, which is followed by minute elastic recovery during subsequent cycles as a result of the reversible compressions of the compressed portion. The poor resilience of bare 3D-foam is owed to the fact that the main effect of compression on them is branch and sheet bending, in which the excellent in-plane strength of graphene/h-BN is not fully utilized.[36] Furthermore, the weak van der Waals intermolecular interactions at the sheet junctions are unable to produce a reversible recovery of the foam after the release of compression loading. These effects lead to the low compressive strength measured.

The notable enhancement in shape recoverability of the "hairy" 3D-foam is quite impressive as only 50% of the space is occupied by the PDMS. This excellent shape recoverability could be attributed to the excellent compressive resilience of the infused PDMS portion and also the bridge-effect of the PDMS between separated graphene sheets which strengthens the whole structure.[39] During the compressive loading and unloading, the restacking and agglomeration of the graphene domains are hindered due to the existence of the PDMS component, which serves as a lubricant that has both glidant and anti-adherent properties. In addition, the more effective and efficient load transfer performance of this hybrid structure and the elasticity of the PDMS portion collectively contribute to the 70-fold increase in compressive strength as compared to the bare 3D-foam (from 0.005 MPa to 0.33 MPa). The overall enhancement in compressive mechanical performance of the hairy 3D-foam ensures its

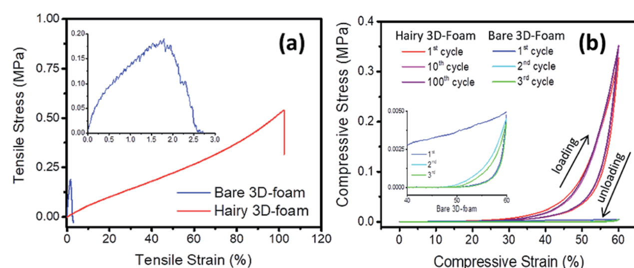

Fig. 6 Mechanical results: (a) stress–strain curves resulting from tensile stress measurements (inset: zoom into the tensile stress–strain curve of bare 3D-foam), (b) cyclic stress–strain curves resulting from compressive stress measurements (inset: zoom into the 40 to 60% compressive strain region of bare 3D-foam).

Open Access Article. Published on 10 August 2017. Downloaded on 7/31/2024 8:21:09 AM.
This article is licensed under a Creative Commons Attribution-NonCommercial 3.0 Unported Licence.

structural stability upon serving as gap filler (*i.e.* withstand possible shock and vibration).

Table 1 summarizes all mechanical test results for the bare 3D-foam and "hairy" 3D-foam. As mentioned previously, under tensile loading, the bare 3D-foams better utilize the high in-plane properties of their constituent 2D-sheets as it aligns towards the direction of the load, and thus the tensile strength is orders of magnitude larger than the compressive strength.

With regard to the "hairy" foam's electrical conductivity, since the outer layers are completely exposed, they completely retain their electrical characteristics (*i.e.* 3D-C remains conductive with $\rho = 1.7\ \Omega$ cm and 3D-BN remains insulating with $\rho = 16.0 \times 10^6\ \Omega$ cm), even during and after bending. This exceeds current best performing 3D-filler/PDMS composites, for example graphene aerogel in PDMS could maximally retain 80% of its electrical conductivity at different bending conditions.[40]

This also applies to the thermal properties of the "hairy" 3D-foams: measurements carried out with the "hairs" fully compressed on both sides of the polymer layer (*i.e.* after being compressed with a force of *ca.* 24 N, which was previously calculated to be the required force to achieve full compression of 3D-foams[18]) achieved similar values as bare fully compressed 3D-foams (*i.e.* ~86 W m^{-1} K^{-1} for 3D-C and ~62 W m^{-1} K^{-1} for 3D-BN). This is more than two orders improvement over previously reported 3D-C/graphene-sheet mixtures (0.7 wt%) in PDMS with 0.56 W m^{-1} K^{-1},[24] and a *ca.* 50-fold and 60-fold increase over 3D-C in epoxy with 1.52 W m^{-1} K^{-1} (ref. 25) and 3D-C/graphene flakes in PDMS with 1.08 W m^{-1} K^{-1},[26] respectively. The hairy method is also able to surpass other high-performance fillers, for example a mixture of PDMS with diamond particles and boron nitride platelets yield 6.1 W m^{-1} K^{-1},[12] 10-times smaller than the 3D-BN "hairy" foam.

These results are evidence that the infused PDMS layer in the centre of the sample does not affect the electrical and thermal transport. This is because the interconnection of the foams is maintained within this layer and the outer bare foam layers are not altered at all. Thanks to this non-invasive method, the phonon and electron transport still takes place on a seamless network and thus the main contribution to the thermal conductivity comes from the 3D-foam. Thus, when the foam is in its compressed state (with the "hairs" fully compressed), the main contribution to the thermal conductivity comes from the bare hairs, and thus the overall thermal conductivity is close to the thermal conductivity of the fully compressed bare foam. This is extremely important for thermal gap filling applications, since this means that the generated heat which is in direct contact with the bottom layer of the foam can be directly transferred through a larger gap into the top layer of the foam which can then be in contact with a cooling section or the ambient to release the heat.

Table 1 Measured mechanical properties

	Bare 3D-foam	Hairy 3D-foam
Tensile strength (MPa)	0.19	0.54
Elongation at break (%)	1.8	102
Young's modulus (MPa)	10.5	0.53
Compressive strength (MPa)	0.005	0.33
Recoverability (%)	~16	~90

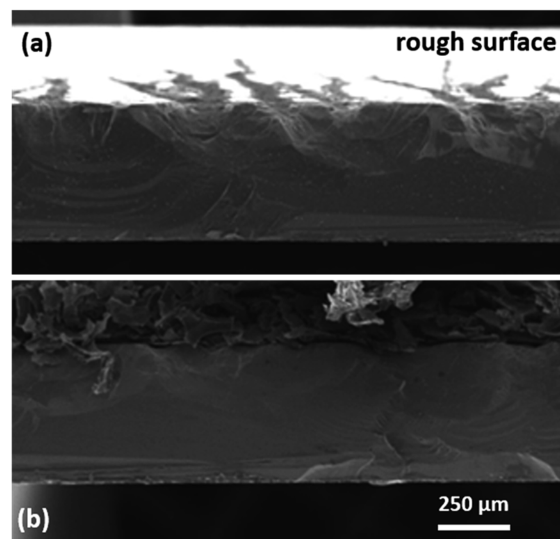

Fig. 7 Surface conformity of the "hairy" 3D-foam: (a) sample rough surface before and (b) after compression with the foam.

Thanks to the exposed hairs, also the same surface conformity as reported for the bare foams is achieved.[18] The amount of exposure of hairs can be tuned in accordance to the surface roughness of the mating surfaces to achieve a seamless contact. Fig. 7a and b show SEM images of a sample rough surface before and after compression with a "hairy" 3D-foam on its surface, respectively. It can be clearly seen how the foam follows exactly the contour of the rough substrate.

It is known that bare 3D-foams remain stable up to 700 °C (3D-C) and 900 °C (3D-BN),[18] but polymers are known to be prone to structural changes at elevated temperatures (*i.e.* above the glass transition temperature T_g, the polymer changes, usually hardens), which could cause thermal expansion mismatches and performance problems.[27] In order to corroborate the applicability of the "hairy" foams for harsh environment thermal management needs

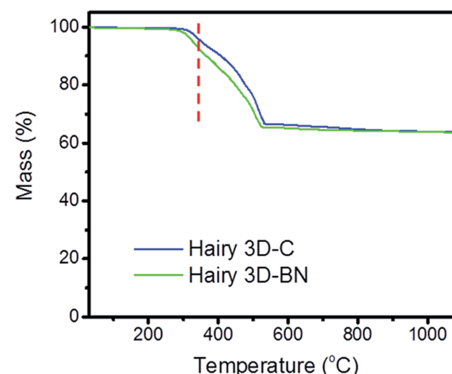

Fig. 8 Thermal stability measurements through thermogravimetric analysis (TGA).

This journal is © The Royal Society of Chemistry 2017

Open Access Article. Published on 10 August 2017. Downloaded on 7/31/2024 8:21:09 AM.
This article is licensed under a Creative Commons Attribution-NonCommercial 3.0 Unported Licence.

(*i.e.* ambient temperatures in the range of 200 °C), its thermal stability was assessed. For this purpose, TGA curves of "hairy" 3D-C and 3D-BN were recorded and are shown in Fig. 8. It can be seen that both the curves follow usual decomposition lines of bare PDMS,[41,42] with a decomposition temperature at around ~330 °C. This remains well above current TIM limits[43] and could thus be used for harsher and more demanding environments, such as electric motors. It must be noted that PDMS is a polymer with intrinsic good environmental stability.[44] Thermal cycling tests previously reported[45] revealed that PDMS can survive in air for long periods at 200 °C and for short periods at 250 °C without degrading. It also retains its flexibility at temperatures down to −45 to −55 °C.[46]

Conclusions

In this work, we have developed a new way of infusing polymer into 3D-foams which leaves the outer parts of the filler still exposed. This method proved to be a very good method to re-inforce the bare 3D-foam structure, since it rendered an increase in tensile strength by ~185%. At the same time, this method allows to fully retain the electrical and thermal characteristics of the foams (electrical resistivity of 1.7 Ω cm for 3D-C and of 16.0×10^6 Ω cm for 3D-BN, thermal conductivity of ~86 W m^{-1} K^{-1} for 3D-C and ~62 W m^{-1} K^{-1} for 3D-BN), since it is a non-invasive way of infusion which preserves the networked and interconnected structure of 3D-foams.

These foams were further characterized according to thermal gap filler needs, which are the compressibility/dampening properties, as well as thermal stability. It was shown that the "hairy" foams provide a restorative force (can act as a spring), with a performance similar to bare PDMS, which is the material currently being used for such purposes. The thermal stability also coincides with bare PDMS, which can withstand temperatures up to 330 °C.

Overall, a new high performance thermal gap filler has been obtained whose collective thermal and mechanical properties enables it to be a viable choice to replace current low-performance gap filler materials, also in harsh environments. This work also provides a new method to hybridize polymers with foam-fillers without the usual encountered detrimental effects.

Conflicts of interest

There are no conflicts of interest to declare.

Acknowledgements

The authors would like to acknowledge the funding support from Singapore Ministry of Education Academic Research Fund Tier 2 No. MOE2013-T2-2-050.

References

1 R. Viswanath, V. Wakharkar, A. Watwe and V. Lebonheur, *Intel Technology Journal Q3*, 2000, 1–16.
2 M. Schulz, *Presented in part at the PCIM*, Nürnberg, 2011, p. 2011.
3 M. Hattori, *High Temperature Electronics, IEEE*, 1999, pp. 37–43.
4 M. R. Fairchild, R. B. Snyder, C. W. Berlin and D. Sarma, Emerging substrate technologies for harsh-environment automotive electronics applications, Report 0148-7191, SAE Technical Paper, 2002.
5 J. Watson and G. Castro, *Analog Dialogue*, 2012, vol. 46, pp. 3–9.
6 M. Ohadi and Q. Jianwei, *Semiconductor Thermal Measurement and Management Symposium, IEEE*, 2004, pp. 231–240.
7 B. A. Myers, *Electronics cooling*, 2003, vol. 9, pp. 24–31.
8 D. Patterson, *COTS Journal*, 2002, 45–48.
9 R. Prasher, *Proc. IEEE*, 2006, **94**, 1571–1586.
10 A. Bar-Cohen, K. Matin and S. Narumanchi, *J. Electron. Packag.*, 2015, **137**, 040803.
11 S. Farhad, D. C. Whalley and P. P. Conway, *Electronics Systemintegration Technology Conference, IEEE proceeding*, 2006, vol. 2, pp. 1292–1302.
12 A. Nakajima, A. Shoji, K. Yonemori and N. Seo, *Jpn. J. Appl. Phys.*, 2016, **55**, 027101.
13 S. Han, D. Wu, S. Li, F. Zhang and X. Feng, *Adv. Mater.*, 2014, **26**, 849–864.
14 B. G. Choi, M. Yang, W. H. Hong, J. W. Choi and Y. S. Huh, *ACS Nano*, 2012, **6**, 4020–4028.
15 A. A. Pesaran, *Battery Man*, 2001, vol. 43, pp. 34–49.
16 R. W. Johnson, J. L. Evans, P. Jacobsen, J. R. Thompson and M. Christopher, *IEEE Trans. Electron. Packag. Manuf.*, 2004, **27**, 164–176.
17 M. R. Werner and W. R. Fahrner, *IRE Trans. Ind. Electron.*, 2001, **48**, 249–257.
18 M. Loeblein, S. H. Tsang, M. Pawlik, E. J. Phua, H. Yong, X. W. Zhang, C. L. Gan and E. H. Teo, *ACS Nano*, 2017, **11**, 2033–2044.
19 Z. Chen, W. Ren, L. Gao, B. Liu, S. Pei and H.-M. Cheng, *Nat. Mater.*, 2011, **10**, 424–428.
20 J. Yin, X. Li, J. Zhou and W. Guo, *Nano Lett.*, 2013, **13**, 3232–3236.
21 M. Loeblein, R. Y. Tay, S. H. Tsang, W. B. Ng and E. H. T. Teo, *Small*, 2014, **10**, 2992–2999.
22 F. Yavari, Z. Chen, A. V. Thomas, W. Ren, H.-M. Cheng and N. Koratkar, *Sci. Rep.*, 2011, **1**, 166.
23 Z. Chen, C. Xu, C. Ma, W. Ren and H.-M. Cheng, *Adv. Mater.*, 2013, **25**, 1296–1300.
24 Y.-H. Zhao, Z.-K. Wu and S.-L. Bai, *Composites, Part A*, 2015, **72**, 200–206.
25 Z. Liu, D. Shen, J. Yu, W. Dai, C. Li, S. Du, N. Jiang, H. Li and C.-T. Lin, *RSC Adv.*, 2016, **6**, 22364–22369.
26 Y.-H. Zhao, Y.-F. Zhang and S.-L. Bai, *Composites, Part A*, 2016, **85**, 148–155.
27 X. C. Tong, *Advanced materials for thermal management of electronic packaging*, Springer Science & Business Media, 2011.
28 S. H. Lee, J. H. Jung and I. K. Oh, *Small*, 2014, **10**, 3880–3886.

Open Access Article. Published on 10 August 2017. Downloaded on 7/31/2024 8:21:09 AM.
This article is licensed under a Creative Commons Attribution-NonCommercial 3.0 Unported Licence.

29 T. Kuilla, S. Bhadra, D. Yao, N. H. Kim, S. Bose and J. H. Lee, *Prog. Polym. Sci.*, 2010, **35**, 1350–1375.
30 L. van der Pauyv, *A method of measuring specific resistivity and Hall effect of discs of arbitrary shape*, 1958.
31 S. Min, J. Blumm and A. Lindemann, *Thermochim. Acta*, 2007, **455**, 46–49.
32 J. Due and A. J. Robinson, *Appl. Therm.*, 2013, **50**, 455–463.
33 N. Goel, T. Anoop, A. Bhattacharya, J. Cervantes, R. K. Mongia, S. V. Machiroutu, H.-L. Lin, Y.-C. Huang, K.-C. Fan and B.-L. Denq, *Thermal and Thermomechanical Phenomena in Electronics Systems, IEEE*, 2008, pp. 248–258.
34 A. C. Ferrari, J. C. Meyer, V. Scardaci, C. Casiraghi, M. Lazzeri, F. Mauri, S. Piscanec, D. Jiang, K. S. Novoselov, S. Roth and A. K. Geim, *Phys. Rev. Lett.*, 2006, **97**, 187401.
35 R. V. Gorbachev, I. Riaz, R. R. Nair, R. Jalil, L. Britnell, B. D. Belle, E. W. Hill, K. S. Novoselov, K. Watanabe, T. Taniguchi, A. K. Geim and P. Blake, *Small*, 2011, **7**, 465–468.
36 A. Nieto, B. Boesl and A. Agarwal, *Carbon*, 2015, **85**, 299–308.
37 F. Liu, P. Ming and J. Li, *Phys. Rev. B: Condens. Matter*, 2007, **76**, 064120.
38 A. Mata, A. J. Fleischman and S. Roy, *Biomed. Microdevices*, 2005, **7**, 281–293.
39 J.-Y. Hong, S. Yun, J. J. Wie, X. Zhang, M. S. Dresselhaus, J. Kong and H. S. Park, *Nanoscale*, 2016, **8**, 12900–12909.
40 B. Song, Z. Wu, Y. Zhu, K.-s. Moon and C. Wong, 2015, **11**, 711–718.
41 G. Camino, S. M. Lomakin and M. Lazzari, *Polymer*, 2001, **42**, 2395–2402.
42 N. Grassie and I. G. Macfarlane, *Eur. Polym. J.*, 1978, **14**, 875–884.
43 http://www.businesswire.com/news/home/20151216005646/en/IDTechEx-Research-More-than-Moore-electronics-packaging, retrieved 16 December 2015.
44 D. Lu and C. Wong, *Materials for advanced packaging*, Springer, 2009.
45 T. Watanabe, N. Ooba, S. Hayashida, T. Kurihara and S. Imamura, *J. Lightwave Technol.*, 1998, **16**, 1049.
46 M. L. Minges, *Electronic materials handbook: packaging*, Asm International, 1989.

 This journal is © The Royal Society of Chemistry 2017